Supporting Information

Ultralong Tumor Retention of Theranostic Nanoparticles with Short Peptide-Enabled Active Tumor Homing

Lihua Li,‡[a] Yao Lu,‡[b] Zefeng Lin,[c] Angelina S. Mao,[d] Ju Jiao,[e] Ye Zhu,[f] Chunyan Jiang,[a] Zhongmin Yang,*[a] Mingying Peng*[a] and Chuanbin Mao*[f]

a. State Key Laboratory of Luminescent Materials and Devices, and Guangdong Provincial Key Laboratory of Fiber Laser Materials and Applied Techniques, School of Physics, School of Materials Science and Engineering, South China University of Technology, 381 Wushan Road, Guangzhou 510641, China.

b. Department of Orthopedics, Zhujiang Hospital, Southern Medical University, Guangzhou, Guangdong 510282, China.

c. Guangdong Key Lab of Orthopedic Technology and Implant, Department of Orthopedics , Guangzhou General Hospital of Guangzhou Military Command, 111 Liuhua Road, Guangzhou, Guangdong 510010, China.

d. Norman North High School, 1809 Stubbeman Ave, Norman, OK 73069, USA

e. Department of Nuclear Medicine, The Third Affiliated Hospital of Sun Yat-sen University, Guangzhou, China, 510630.

f. Department of Chemistry and Biochemistry, Stephenson Life Sciences Research center, Institute for Biomedical Engineering, Science and Technology, University of Oklahoma, Norman, OK 73019, USA.

‡ Lihua Li and Yao Lu contributed equally to this work.

*Corresponding authors: Zhongmin Yang, Mingying Peng and Chuanbin Mao. (*email: yangzm@scut.edu.cn, pengmingying@scut.edu.cn, cbmao@ou.edu)

Supplementary Experiment Section

Materials. Bismuth (Ⅲ) nitrate pentahydrate ($Bi(NO_3)_3 \cdot 5H_2O$), tetraethyl orthosilicate (TEOS), gadolinium chloride ($GdCl_3$), 1-dodecanethiol, 3-(4,5-dimethylthiazol-2-yl)-2,5-diphenyltetrazolium bromide (MTT), aminopropyltriethoxysilane (APTES), succinic anhydride, PEG-NH_2 (MW=2500), cyclohexane and other chemicals were purchased from Aladdin (Shanghai, China). The peptides used in further conjugation with the nanocomposites were synthesized with four glycine amino acids (GGGG) and four additional lysine amino acids (KKKK) at the C-terminal. The targeted AR peptides (AREYGTRFSLIGGYR) selected in our previous study[1] and random peptides (EARGFSLGYRIYGRT) were purchased from Wuhan Haode Peptide Co., Ltd. (Wuhan, China). NHS-fluorescein, doxorubicin hydrochloride (DOX), Calceine AM and PI were purchased from Sigma-Aldrich (St. Louis, MO).

Synthesis of the multifunctional nanocomposites. The Bi NPs were synthesized by following a previous report.[2] Bi@SiO_2 NPs were synthesized by a reverse microemulsion approach. Briefly, 20 mg Bi NPs were dispersed in 100 mL cyclohexane treated with ultrasonication for 30 min. 5 mL polyoxyethylene (5) nonylphenylether (Igepal CO-520) was mixed with 10 mL cyclohexane uniformly and added to the above solution. After the mixture was stirred at room temperature for 30 min, 1 mL concentrated ammonia aqueous solution (28%, 2.8 mL) was added and stirred for another 30 min. Subsequently, 50 μL TEOS dissolved in 6.5 mL cyclohexane was added to initiate silica shell growth. After stirring for 24 h in room

temperature, the products were separated by centrifugation and washed with ethanol and water each for 3 times. The products were denoted as $Bi@SiO_2$.

Preparation of $Bi@SiO_2$-Gd and AR-$Bi@SiO_2$-Gd. 7 mg $Bi@SiO_2$ was resuspended in 7 mL distilled water. The Gd-DTPA stock solution (100 mg/mL, 80 μL) was added to $Bi@SiO_2$ solution and agitated for 15 min. TEOS (20 μL, in ethanol) was then added to the solution, followed by heating the solution for 5 min to raise its temperature to 40 ºC. After NH_4OH (0.6 mL, 25 wt.%) was added to the solution, the resultant solution was aged at 40 ºC for one day. The products were isolated from the solution by centrifugation and rinsed with water and ethanol. The products were termed $Bi@SiO_2$-Gd NPs.

20 mg of the resultant $Bi@SiO_2$-Gd NPs was dispersed in 20 mL absolute ethanol, to which 1 mL APTES was added to form a product termed $Bi@SiO_2$-Gd-NH_2. $Bi@SiO_2$-Gd-COOH was produced by the conjugation of the succinic anhydride to $Bi@SiO_2$-Gd-NH_2 in the presence of a catalyst (triethylamine) via a nucleophilic ring opening reaction. The AR peptide was then conjugated with $Bi@SiO_2$-Gd-COOH according to our previous protocol to form AR-$Bi@SiO_2$-Gd.[3]

Characterization. The crystalline structure, size and shape of the nanoparticles were observed by X-ray diffraction (XRD) and high-resolution transmission electron microscopy (HRTEM). XRD was measured with a Siemens Kristalloflex 810 D-500 X-ray diffractometer (Karslruhe, Germany) under an operating mode of 40 kV and 30 mA, with λ = 1.5406 Å radiation. Bi, $Bi@SiO_2$, $Bi@SiO_2$-Gd NPs in solution were placed onto holey carbon-covered copper grids for high resolution transmission

electron microscopy (HRTEM) observation. The HRTEM images, high-angle annular dark-field scanning TEM (HAADF-STEM) image and element mapping were obtained from the particles with a Hitachi 2100 electron microscope with an accelerating voltage of 210 KV. Fourier transform infrared spectroscopy (FTIR) spectra were measured on a PerkinElmer 580B IR spectrophotometer using the KBr pellet technique. N_2 adsorption/desorption isotherms were obtained on a Micromeritics ASAP Tristar II 3020 apparatus. Zeta potential and hydrophilic size measurements were determined with the Zetasizer Nano Z (Malvern, UK). UV-vis-NIR absorption spectra were measured by the multifunctional microplate reader (Thermo, USA). Pore size distribution was calculated by the Brunauer-Emmett-Teller (BET) method. To determine the AR content in AR-Bi@SiO_2-Gd, the synthesized Bi@SiO_2-Gd-AR NPs were first dialyzed in dialysis tube (MW=3500) to remove any impurities, and then centrifugated to collect the supernatant. Then the residual peptides were quantified using a BCA assay kit and thus the content of the conjugated AR peptide in unit mass of NPs (μg mg^{-1}) could be further determined.

Drug loading and release. 10 mg AR-Bi@SiO_2-Gd were suspended in 10 mL PBS to form a solution. Then 5, 10 mg DOX was separately dissolved in the solution, followed by stirring overnight. The resultant solution was centrifuged and washed with PBS solution to get rid of the free DOX. The absorbance at 482 nm was measured to determine the DOX amount in the supernatant solutions. The following formula was used to determine the encapsulation efficiency:

Encapsulation efficiency% = weight of DOX loaded to NPs/initial DOX weight ×100 %.

To evaluate the DOX release under different pH values, 5 mg AR-Bi@SiO_2-Gd /DOX NPs were suspended in 5 mL PBS solution (pH=5.0, 7.4). After the solution was continuously stirred at 37 ºC and centrifuged, the supernatant solution was collected and its absorbance at 482 nm was measured at different time points (0, 0.5, 1, 4, 8, 12, 24 h).

***In vitro* AR-Bi@SiO_2-Gd targeting effect.** The FITC labeled AR-Bi@SiO_2-Gd, CP-Bi@SiO_2-Gd, PEG-Bi@SiO_2-Gd and free FITC were co-cultured with MCF-7 cells for 24 h, respectively. For the blocking group, 2.35 μg free AR peptide (in equivalent amount as the peptide in the AR-bearing NPs) was first co-cultured with MCF-7 cells for 3 h, and then the FITC-labeled AR-Bi@SiO_2-Gd NPs were added and co-cultured with these cells for addiitonal 24 h. The cells were washed to allow the free NPs to be removed and imaged under a fluorescence microscope. Flow cytometry analysis of the cells was done to verify the NP targeting effect. To further confirm the selectivity targeted effect, we also co-cultured the FITC labeled NPs with other types of breast cancer cell lines (MDA-231 and SKBR-3) and normal breast MCF-10A cells, and then imaged the cells using a fluorescence microscope.

The toxicity and in vitro photothermal-chemotherapy of the NPs. For toxicity analysis, breast cancer cells MCF-7, MCF-10A were seeded on the plates at a density of 5×10^4 cells per cm^2 seprately and cultured at 37 ºC, 5% CO_2 using DMEM culture with 10% fatal bovine overninght. Then AR-Bi@SiO_2-Gd with a gradient

concentration of 0, 15.625, 31.25, 62.5, 125, 250, 500 μg/mL was separately added to the plates. After the cells were co-cultured for 24 h, the MTT test was performed to evaluate cell viability. The PEG-Bi@SiO_2-Gd, AR-Bi@SiO_2-Gd and CP-Bi@SiO_2-Gd loaded with or without DOX were cultured with MCF-7 cells for another 6 h. Then the cells were washed with PBS for three times and replaced with fresh medium and irradiated with 808 nm laser (1 W/cm^2 or 0 W/cm^2) for 5 min. The standard MTT assay was carried out to determine the cell viabilities relative to the untreated control cells. The hemocompatibility of the AR-Bi@SiO_2-Gd was evaluated by hemolysis ratio.

Live/Dead staining. 5 × 10^4 cells/cm^2 breast cancer MCF-7 cells were seeded on 96-well plates at 37 °C with 5 % CO_2 for 24 h. 100 μL of PEG-Bi@SiO_2-Gd/DOX, AR-Bi@SiO_2-Gd, AR-Bi@SiO_2-Gd/DOX and CP-Bi@SiO_2-Gd/DOX NPs were added to the plate, then irradiated with NIR laser (808 nm, 1 W/cm^2) for 5 min. After co-cultured for 24 h, the cells were subject to Live/Dead staining following the manufacturer's protocol (Sigma, USA) and imaged under a fluorescence microscope (DMI4000, Leica). Similarly, the same procedure was carried out on normal breast MCF-10A cells.

Animals. Balb/c nude mice (six-week-old, female) were used in this study. The protocol was approved by Institutional Animal Care and Use Committee of Guangzhou General Hospital.

***In vitro* and *in vivo* CT imaging.** The Bi@SiO_2-Gd NPs solution was diluted with a serial concentration (50, 25, 12.5, 6.25, 3.125 mg/mL). The NPs solutions were placed

into a 24-well plate under X-ray scanning in order to measure the HU value. 5×10^6 MCF-7 cells in PBS were then injected into the thymus gland of the mice to establish tumor model. After two weeks, 200 μL of NPs (AR-Bi@SiO_2-Gd, CP-Bi@SiO_2-Gd, or PEG-Bi@SiO_2-Gd, equivalent to 10 mg/kg Bi@SiO_2-Gd) were *i.v.* injected into the tumor model. 3 h, 24 h, 4 d, 10 d, 7 d and 14 d post-injection, the CT images of the tumor-bearing mice were collected under a small animal X-ray CT scanner. Moreover, the CT images were also collected on day 1, 4, and 7 post treatment during the cancer treatment process.

***In vitro* and *in vivo* MRI.** A 3-T clinical MRI instrument was used to collect the T_1-weighted MR images and measure the relaxation time from the NP solutions at different Gd concentrations (0, 0.05, 0.1, 0.2, 0.4, 0.8 mM) (dispersed in 1% agarose gel). The standard Gd-DTPA was dissolved in a gradient concentration of 0, 0.02, 0.04, 0.08, 0.16, 0.32, 0.64 mM and set as a control. The slope of the dependence of relaxation rate $1/T_1$ (s^{-1}) on the Gd^{3+} concentration of (mM) was used to determine the r_1 relaxivity value. For *in vivo* MRI, the mice were anesthetized and then intravenously injected with PEG-Bi@SiO_2-Gd, CP-Bi@SiO_2-Gd and AR-Bi@SiO_2-Gd. MR imaging was then done on the animals at different time points post-injection of NPs (same time points as in CT imaging). The monitoring also proceeded on day 1, 4 and 7 during tumor treatment (AR-Bi@SiO_2-Gd/DOX + NIR) process.

***In vivo* tumor therapy.** After the tumors grew to reach a diameter of 0.5-0.7 cm, 7 random groups (n=4) of mice were undergoing different treatments: 1)

AR-Bi@SiO_2-Gd/DOX + NIR; 2) AR-Bi@SiO_2-Gd + NIR; 3) AR-Bi@SiO_2-Gd/DOX; 4) CP-Bi@SiO_2-Gd/DOX + NIR; 5) PEG-Bi@SiO_2-Gd/DOX + NIR; 6) DOX only + NIR; and 7) Control group (sodium chloride + NIR). The temperate change of the tumors was monitored by infrared (IR) imaging. The size of the tumors was measured every other day for two weeks. Then the tumors were histologically analyzed by hematoxylin and eosin (H&E) staining.

Biodistribution, metabolism and clearance. The MCF-7 tumor-bearing nude mice were randomized into 3 groups (n=4). Then the mice were given 200 μL of AR-Bi@SiO_2-Gd, CP-Bi@SiO_2-Gd, or PEG-Bi@SiO_2-Gd (10 mg/kg) through *i.v.* injection. The main organs (spleen, lung, heart, liver, and kidney), peritumoral muscle, and tumors were obtained from the animals and digested with HNO_3:HCl (3:1) after 24 h, the Bi/Gd content in each sample was analyzed using ICP-MS. In addition, we investigated the metabolism behavior of AR-Bi@SiO_2-Gd in detail. Briefly, the main organs, peritumoral muscle, tumors, blood, urine and faeces were collected at different time points post-injection of AR-Bi@SiO_2-Gd. To evaluate the half time in blood and tumor, the Bi and Gd content in blood and tumors at different time points were also analyzed by ICP-MS.

Blood analysis. Balb/c mice were intravenously injected with AR-Bi@SiO_2-Gd (10 mg/kg) for 1, 4, 7 days, and then the blood was collected and subjected to blood routine and liver and kidney function assays. Mice injected with normal saline were set as a control group.

The stability of Bi@SiO_2-Gd NPs. The stability of Bi@SiO_2-Gd NPs was evaluated by the Bi^{3+} and Gd^{3+} ions in simulated body fluid (SBF) solution, PBS (pH 7.4), normal saline. Breifly, 10 mg Bi@SiO_2-Gd NPs were dispersed in 10 mL SBF solution. Then the amount of Gd^{3+} ions in the solution was monitored by ICP-MS.

Statistical Analysis. Data were analyzed by SPSS 19.0 software (IBM, USA). Statistical comparisons among multiple treatment groups were measured using one-way analysis of variance (ANOVA) followed by post hoc multiple comparison (LSD test). The results were presented as means ± standard deviation. A *p*-value less than <0.05 was regarded as statistically signifcant.

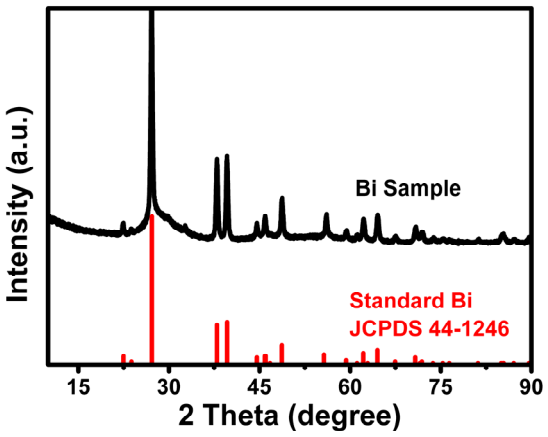

Figure S1. The XRD patterns of the as-synthesized Bi (inner core) nanoparticles.

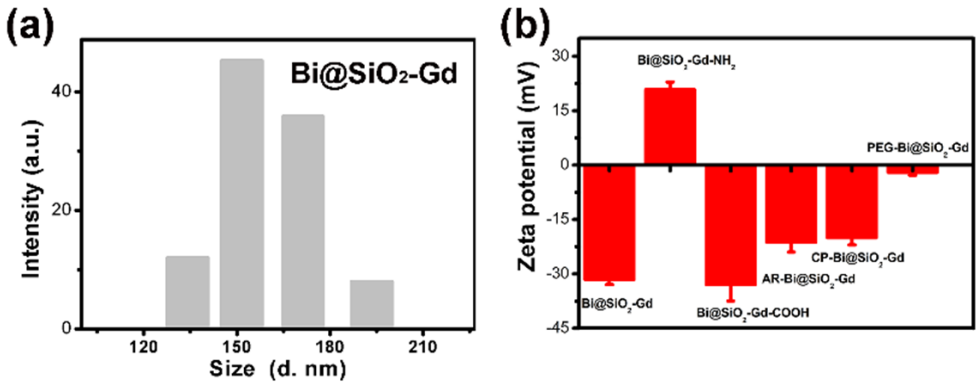

Figure S2. (a) Size distribution of the as-synthesized Bi@SiO_2-Gd; (b) Zeta potentials of the Bi@SiO_2-Gd, Bi@SiO_2-Gd -NH_2, and AR-Bi@SiO_2-Gd.

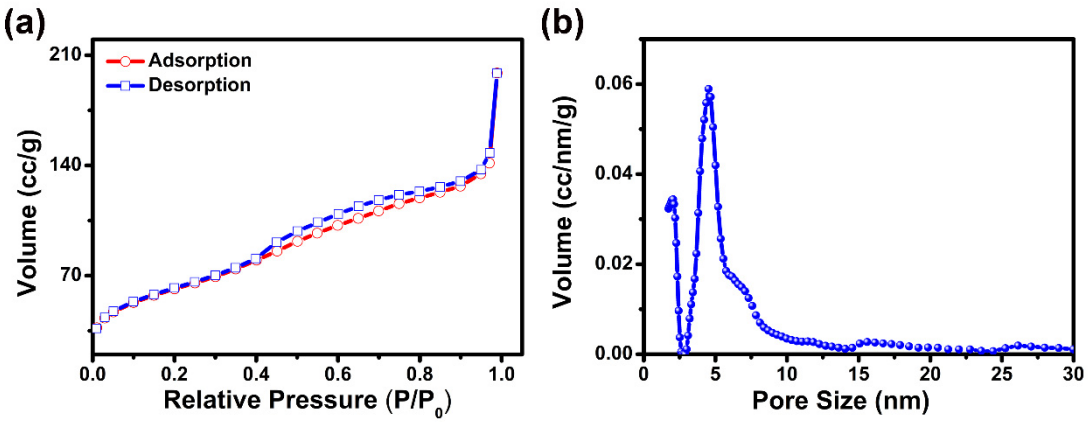

Figure S3. (a) Nitrogen adsorption/desorption isotherms of Bi@SiO_2-Gd NPs. (b) Pore size distributions of Bi@SiO_2-Gd NPs.

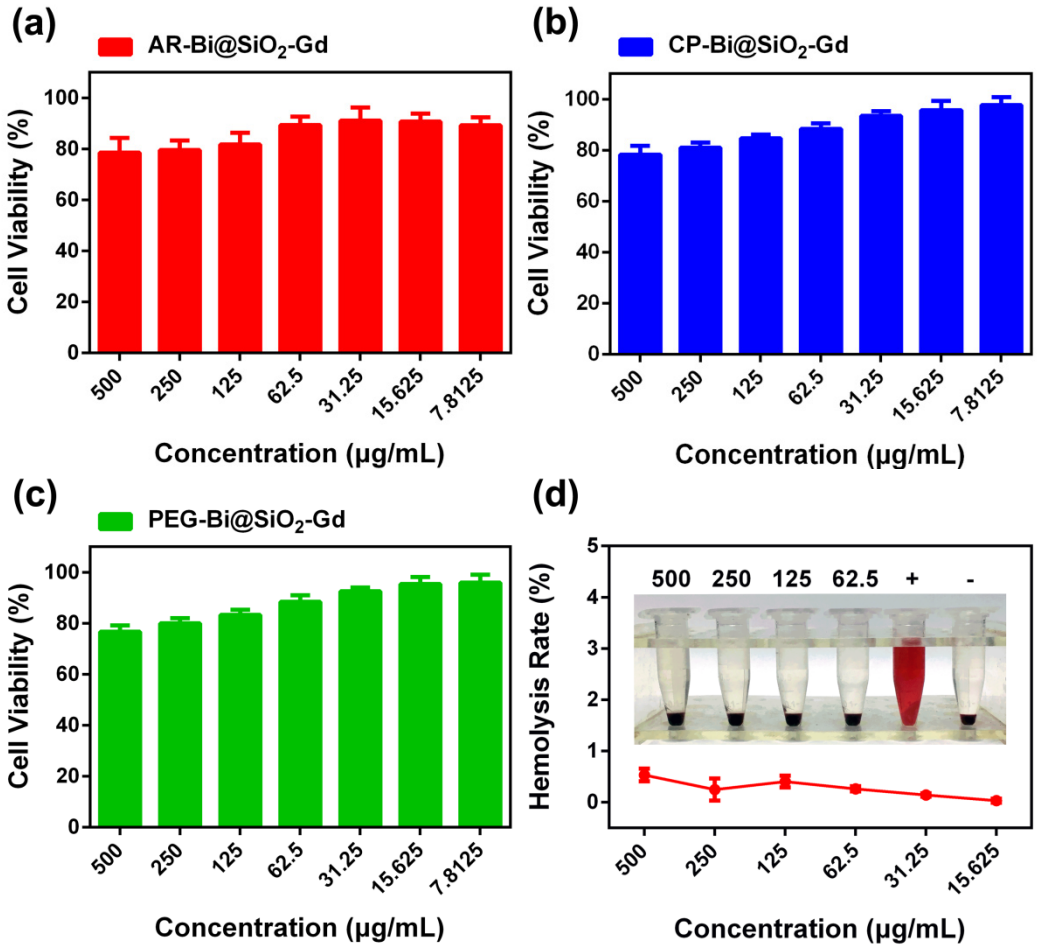

Figure S4. Biocompatibility and blood compatibility of the AR-Bi@SiO_2-Gd. (a-c) Cell viability of MCF-7 cells after being cultured with different concentrations of (a) AR-Bi@SiO_2-Gd; (b) CP-Bi@SiO_2-Gd; (c) PEG-Bi@SiO_2-Gd. (d) Hemolysis rate of blood after being co-cultured with different concentrations of the AR-Bi@SiO_2-Gd (500, 250, 125, 62.5, 31.25, 15.625 μg/mL). Inset picture presents the blood cells co-cultured with gradient concentrations of the NPs (500, 250, 125, 62.5 μg/mL), dd H_2O water (+), and PBS (-) after centrifugation. The transparent supernatant in the NPs group suggests the good blood compatibility of the Bi@SiO_2-Gd.

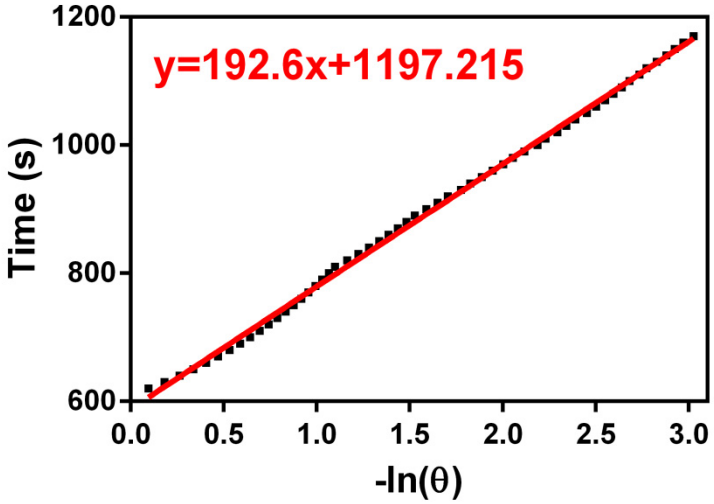

Figure S5. Time constant for heat transfer from the system is determined to be τ= 322 s by linear fitting of time versus negative natural logarithm of driving force temperature (-ln) during the cooling stage in Figure 1(h).

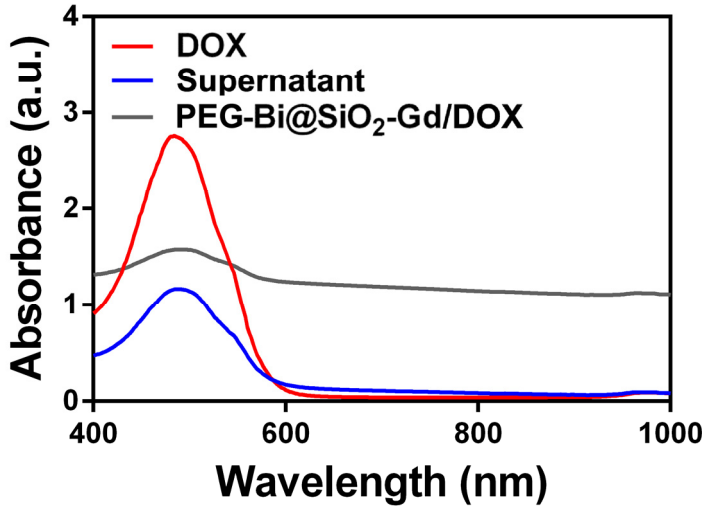

Figure S6. DOX loading efficiency on PEG-Bi@SiO_2-Gd.

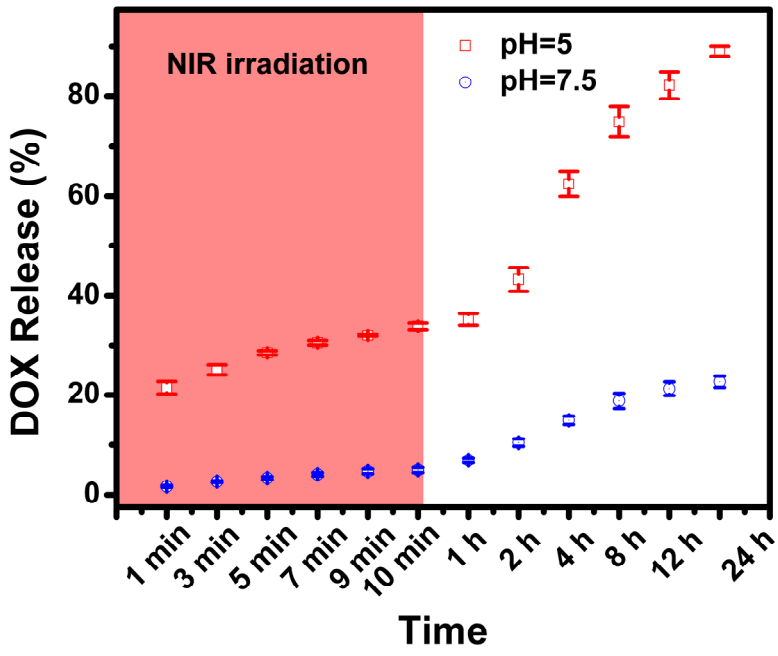

Figure S7. Drug release curve during and after NIR irradiation (808 nm, 5 min) from AR-Bi@SiO_2-Gd/DOX at acidic (pH 5) and neutral (pH 7.4) conditions. The left shaded area is for during the NIR irradiation.

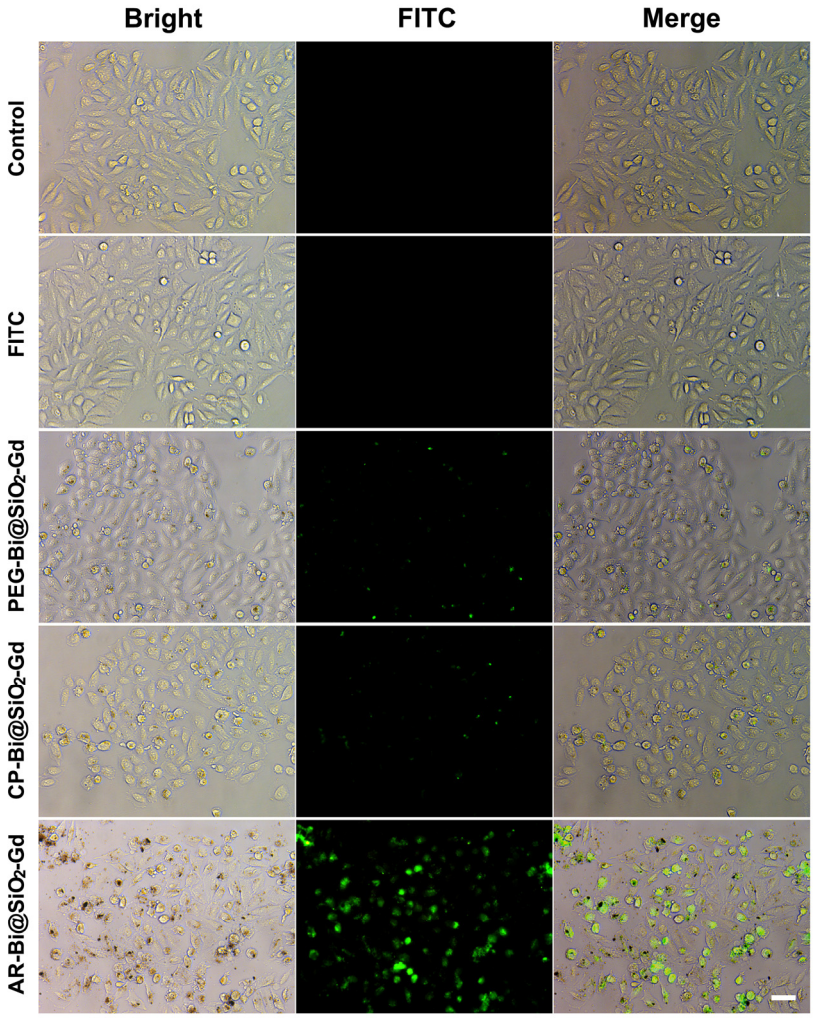

Figure S8. Fluorescence images of MCF-7 cells co-cultured with free FITC as well as FITC-labeled PEG-Bi@SiO_2-Gd, CP-Bi@SiO_2-Gd and AR-Bi@SiO_2-Gd. The results indicated excellence targeted effect of AR-Bi@SiO_2-Gd on MCF-7 breast cancer cells. Scale bar= 50 μm.

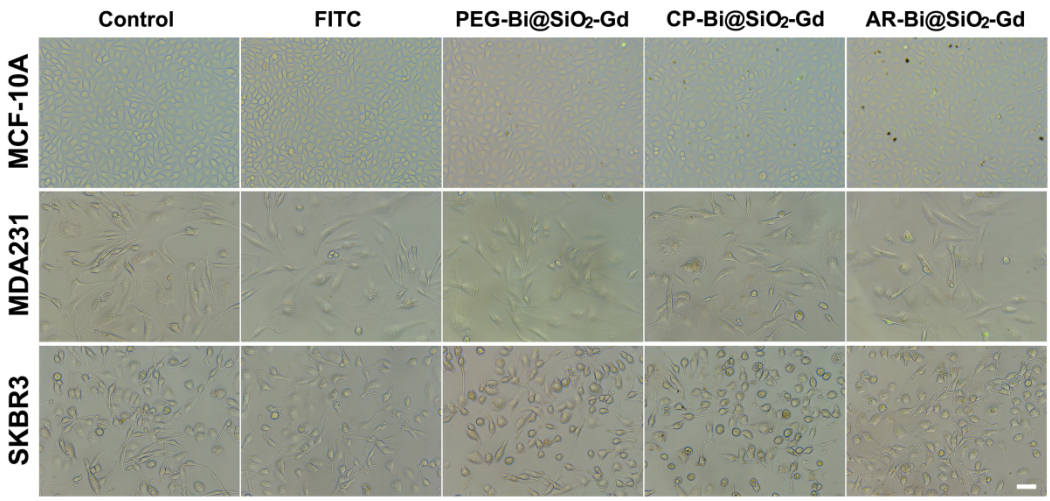

Figure S9. Merged fluorescence images of MCF-10A, MDA-231 and SKBR-3 cells co-cultured with free FITC as well as FITC-labeled PEG-Bi@SiO_2-Gd, CP-Bi@SiO_2-Gd and AR-Bi@SiO_2-Gd. The results indicated negligible targeted effect of AR-Bi@SiO_2-Gd on normal breast cells and the other breast cancer cells. Scale bar= 50 μm.

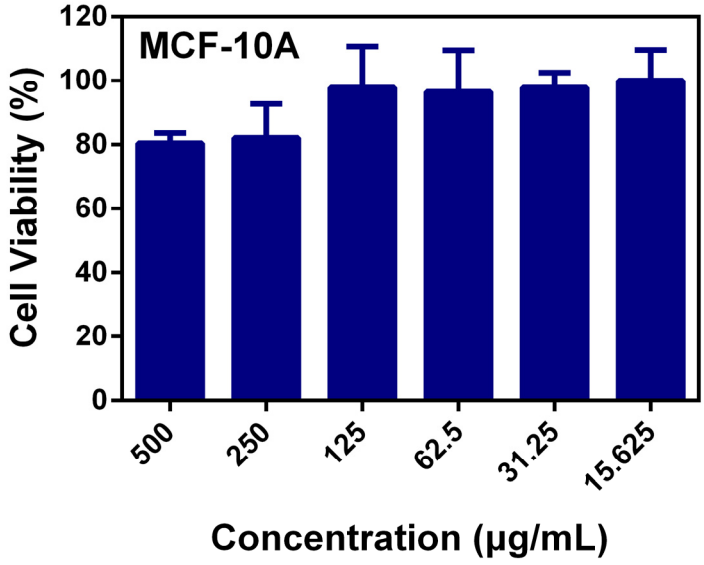

Figure S10. Cell viability of MCF-10A cells (normal breast cells) after being cultured with different concentrations of AR-Bi@SiO_2-Gd.

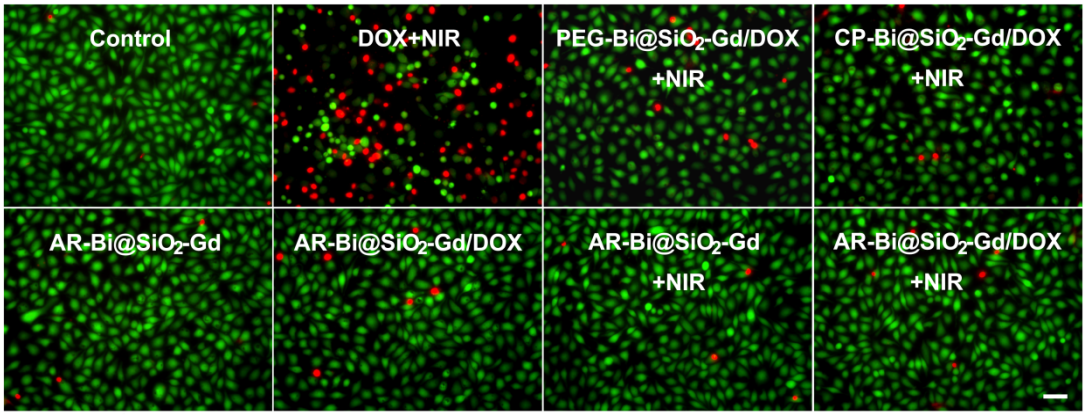

Figure S11. Live/dead staining of MCF-10A cells after co-cultured with different NPs, the results indicated negligible toxicity on normal breast cells of NPs due to the negligible targeting effect of AR-Bi@SiO_2-Gd on MCF-10A cells and almost no drug release in the neutral solution. Scale bar= 50 μm.

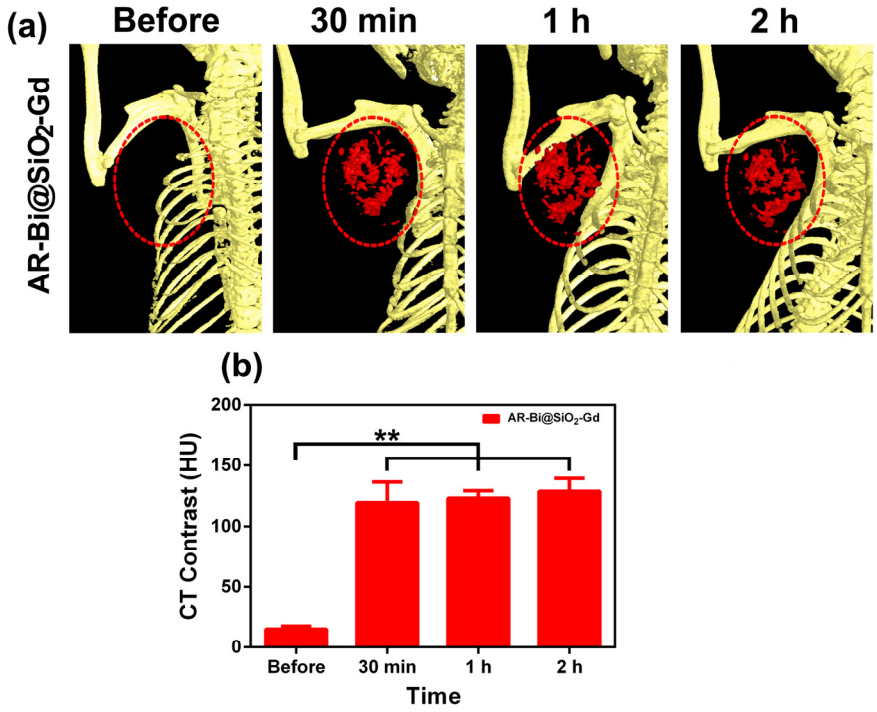

Figure S12. CT iamging of AR-Bi@SiO_2-Gd on breast cancer bearing mice before injection and at 30 min, 1 h and 2 h post injection. (a) CT contrast images at 30 min, 1 h, 2 h after single injection of AR-Bi@SiO_2-Gd through tail vein. (b) Changes of the CT contrast in (a). The results indicate that the AR-Bi@SiO_2-Gd NPs can monitor the tumor during the early stage. **$p < 0.01$.

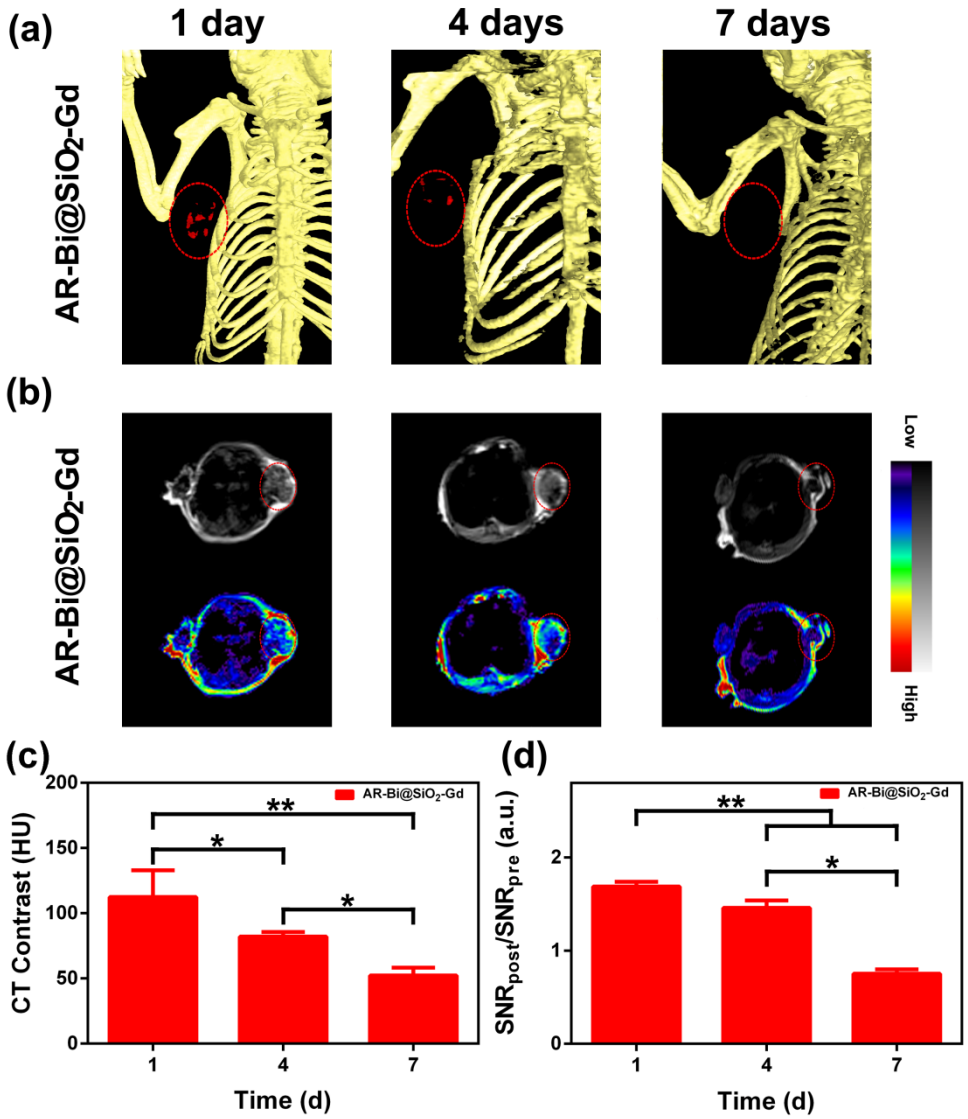

Figure S13. Long-term monitoring of breast tumors during tumor treatment process using CT & MRI. (a) CT contrast images and (b) coronal T_1-weighted MRI images 1, 4 and 7 days after AR-Bi@SiO_2-Gd/DOX+NIR treatment. (c-d) Changes of (c) the CT contrast and (d) the signal-to-noise ratio from T_1-weighted MRI images at the tumor site. The results illustrate the AR-Bi@SiO_2-Gd NPs monitor the tumor during treatment. *$p < 0.05$, **$p < 0.01$.

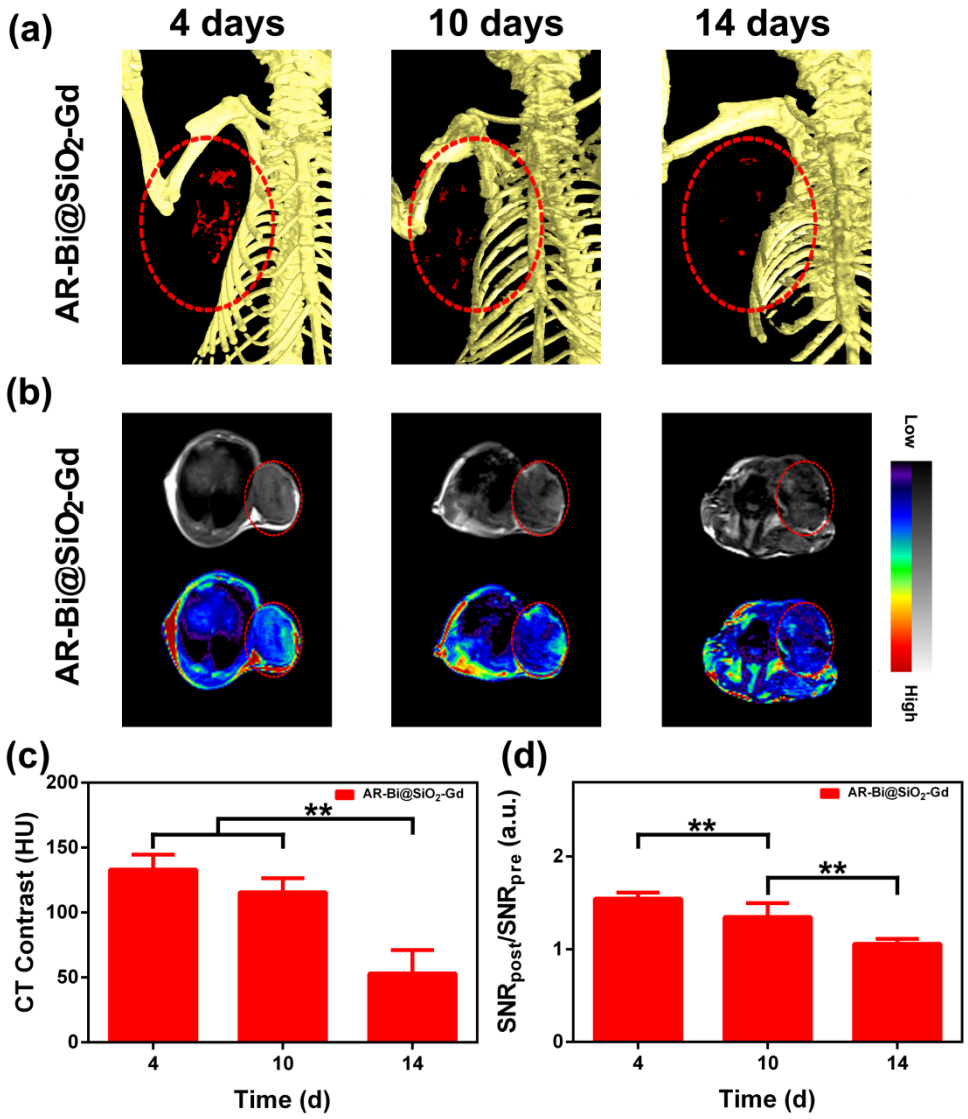

Figure S14. Long-term monitoring ability of AR-Bi@SiO_2-Gd. (a) CT contrast images and (b) coronal T_1-weighted MRI images 4, 10, 14 days after single injection of AR-Bi@SiO_2-Gd. (c-d) Changes of the CT contrast (c) and the signal-to-noise ratio from T_1-weighted MRI images (d) at the tumor site. The results indicate that the AR-Bi@SiO_2-Gd NPs can monitor the tumor for a long period. *$p < 0.05$, **$p < 0.01$.

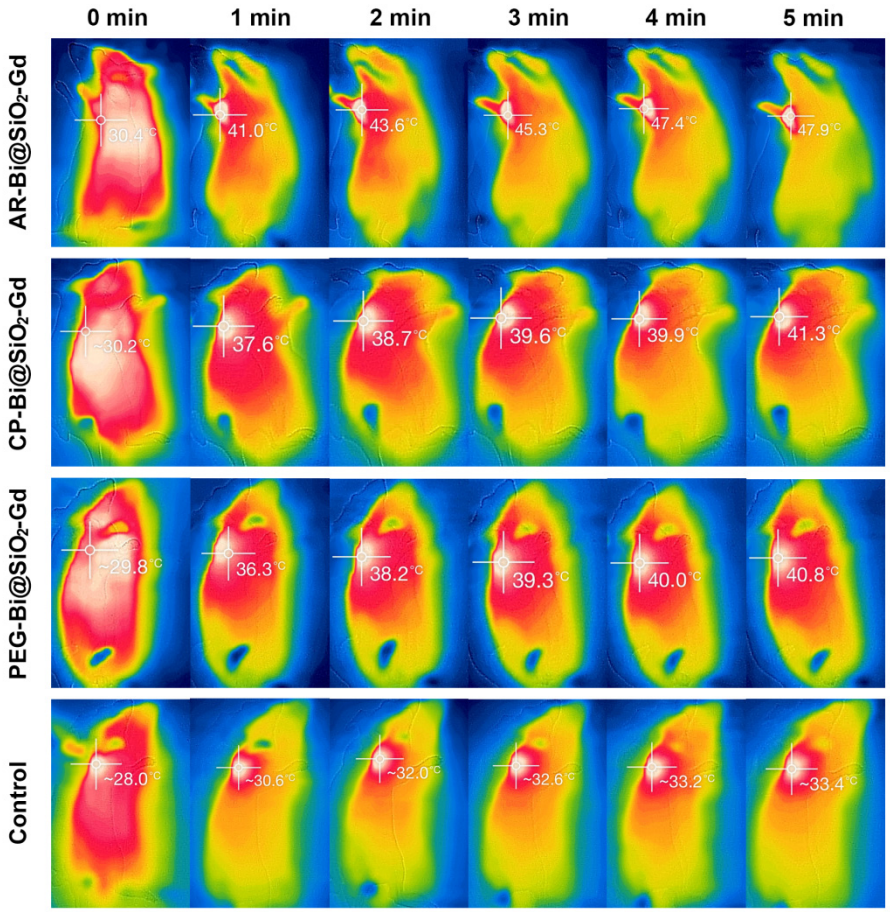

Figure S15. IR images of the animals captured every 1 min (from left to right) showing the temperature change at the tumor sites under 1 W/cm^2 808 nm laser irradiation.

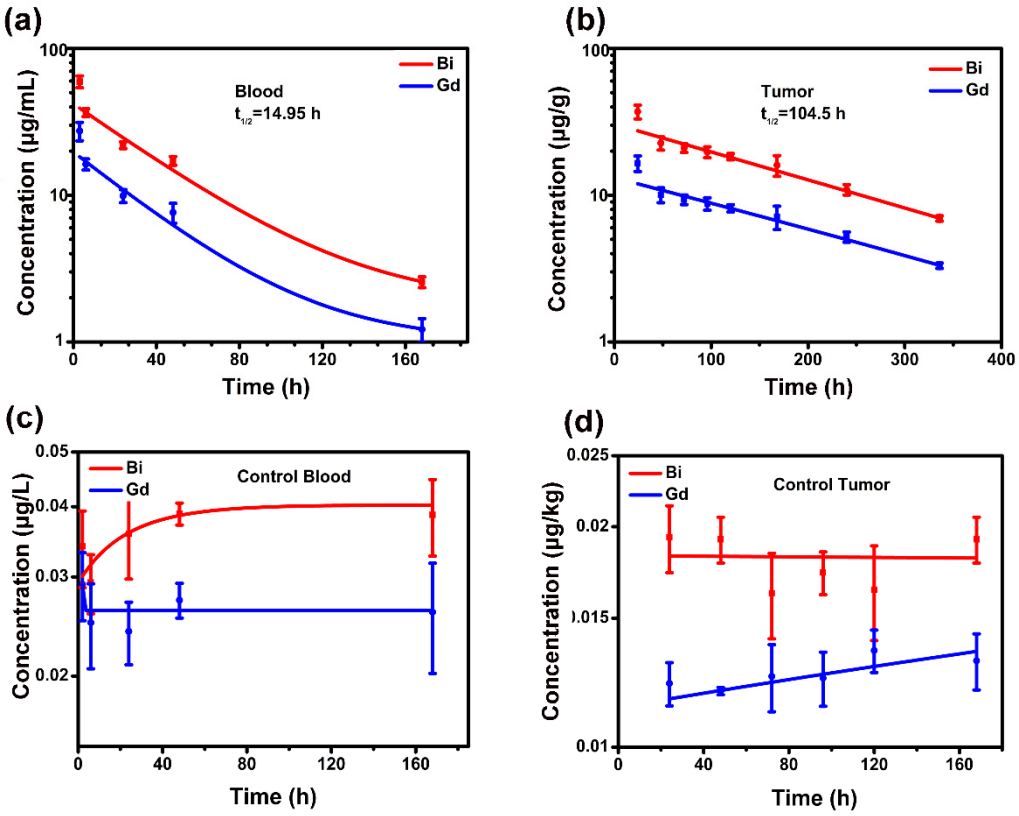

Figure S16. The dynamic changes of Bi and Gd contents in blood and tumor at different time intervals. (a-b) The AR-Bi@SiO_2-Gd half-life in (a) blood was 14.95 h and (b) tumor was 104.5 h, respectively. (c-d) The corresponding dynamic changes of Bi and Gd contents in (c) blood and (d) tumor at different time intervals in control group.

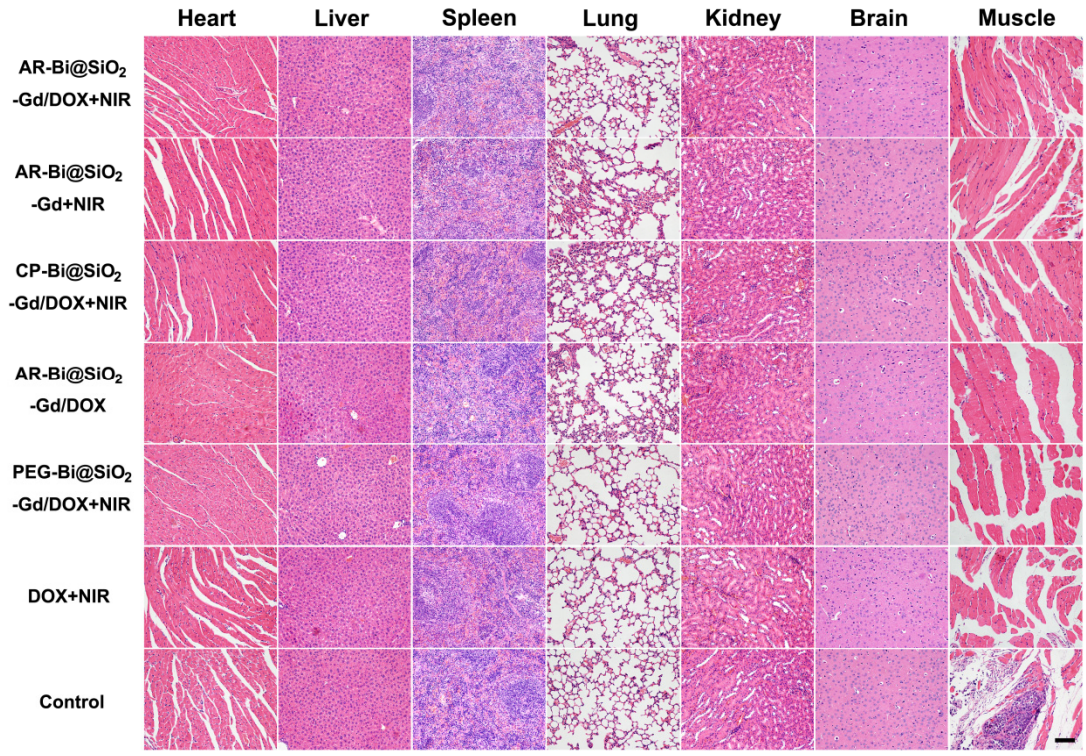

Figure S17. H&E stainning of the main organs in different treatment groups. Scale bar= 200 μm.

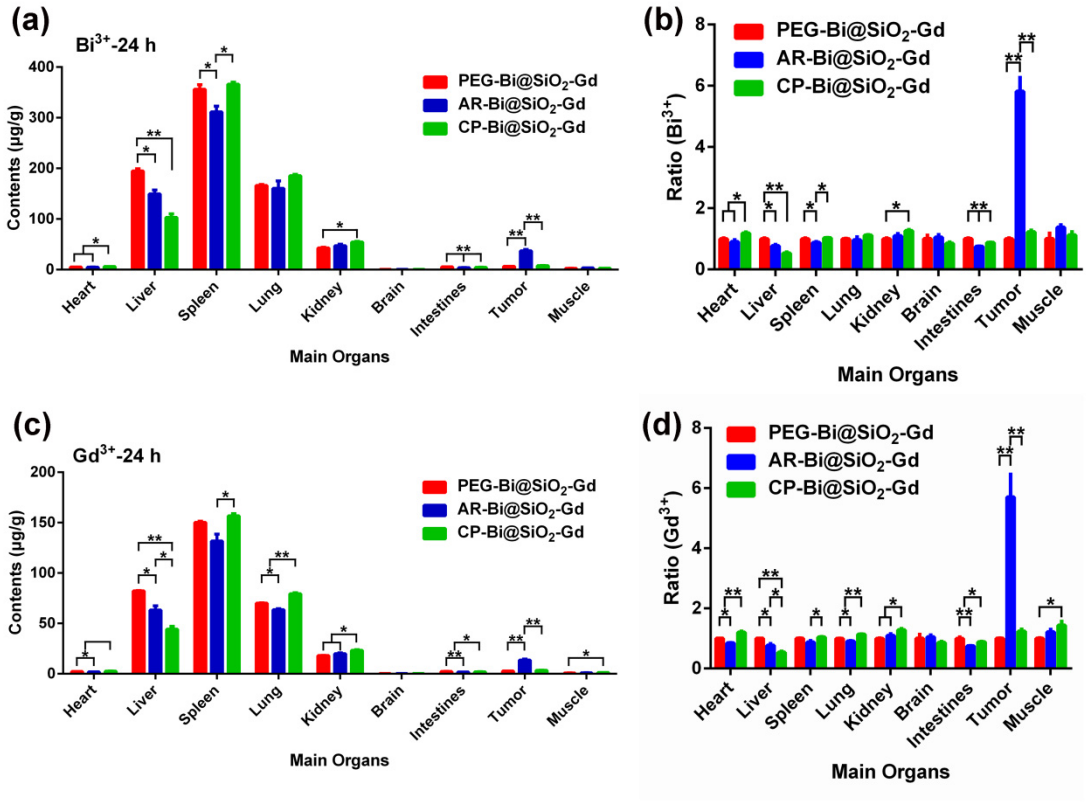

Figure S18. Organ ditribution of Bi^{3+} (a) and Gd^{3+} (c) in AR-Bi@SiO_2-Gd, CP-Bi@SiO_2-Gd and PEG-Bi@SiO_2-Gd groups after i.v injection of 24 h. (b) and (d) are derived from (a) and (c), respecitively, by normaling the amount of Bi or Gd in different groups to that in the PEG-Bi@SiO_2-Gd group. The data indicate that the AR-Bi@SiO_2-Gd could more effectively accumulate in the tumor site than the other groups. *$p < 0.05$, **$p < 0.01$.

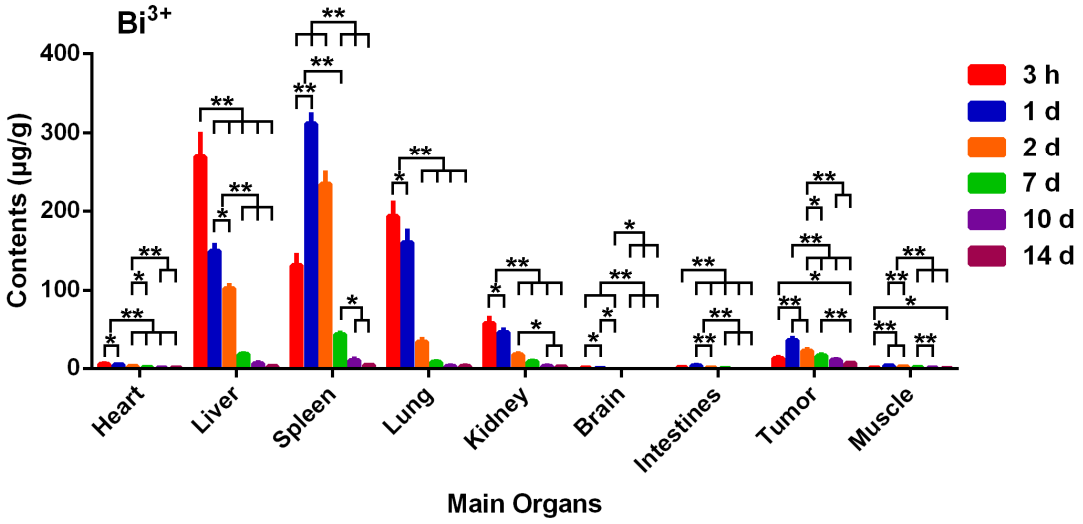

Figure S19. The dynamic change of Bi in the main organs after i.v injection of AR-Bi@SiO_2-Gd. The data indicate that the tumor-targeting AR-Bi@SiO_2-Gd could effectively accumulate in the tumor site and lasted for more than 7 days. *$p < 0.05$, **$p < 0.01$.

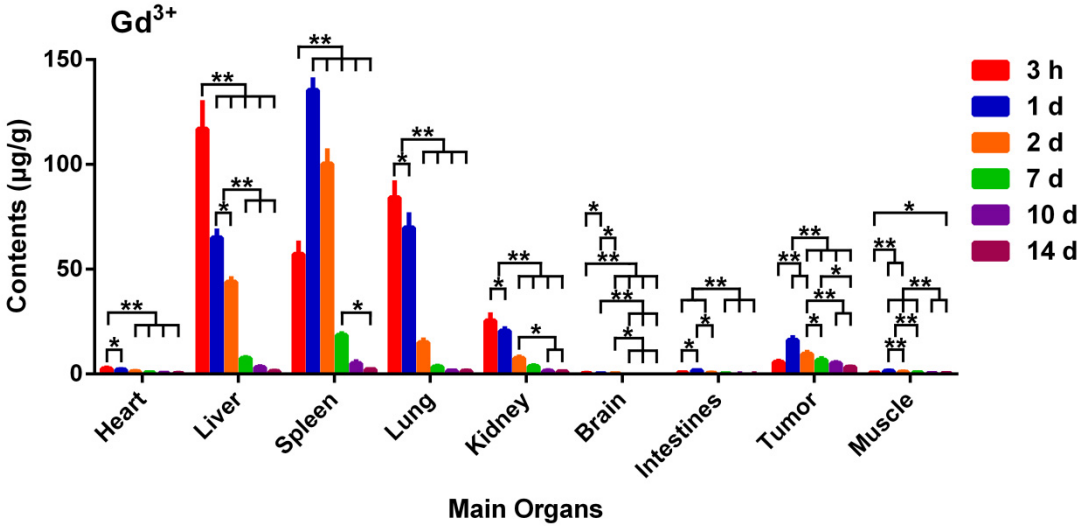

Figure S20. The dynamic change of Gd in main organs after i.v injection of AR-Bi@SiO_2-Gd. The data indicate that the tumor-targeting AR-Bi@SiO_2-Gd could effectively accumulate in the tumor site and lasted for more than 7 days. *$p < 0.05$, **$p < 0.01$.

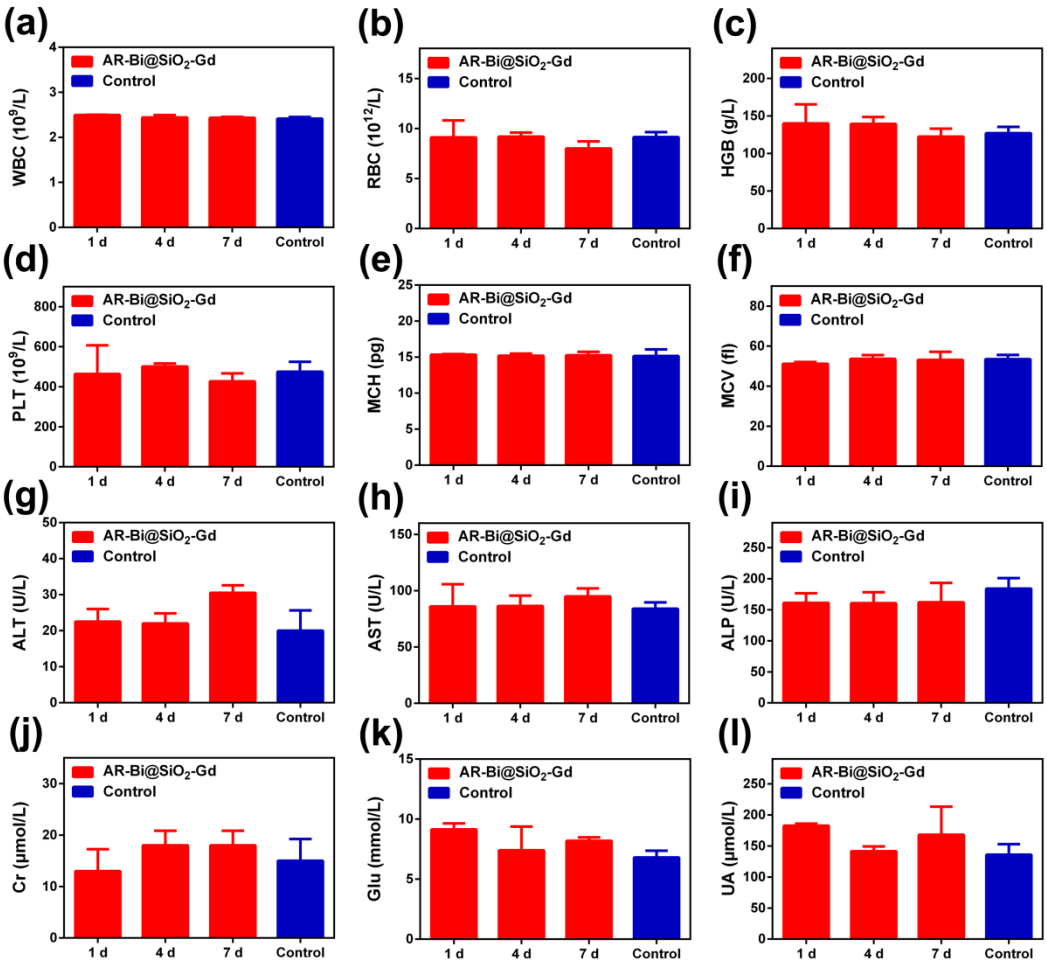

Figure S21. Blood routine & biochemical analysis. (a) White blood cell (WBC); (b) Red blood cell (RBC); (c) Hemoglobin (HGB); (d) Platelet (PLT); (e) Mean corpuscular hemoglobin (MCH); (f) Mean corpuscular volume (MCV); (g) Alanine aminotransferase (ALT); (h) Aspartate aminotransferase (AST); (i) Alkaline phosphatase (ALP); (j) Creatinine (Cr) ; (k) Glucose (Glu); (l) Uric acid (UA).

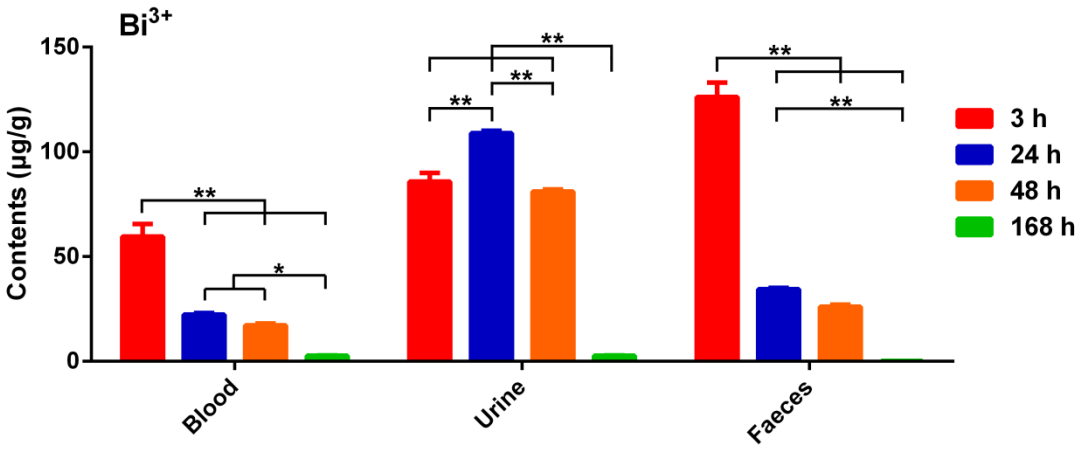

Figure S22. The dynamic change of Bi in blood, urine and faeces after i.v injection of AR-Bi@SiO_2-Gd. The data indicate that the tumor-targeting AR-Bi@SiO_2-Gd could be expeled from the body through urine and faeces after 7 days. *p < 0.05, **p < 0.01.

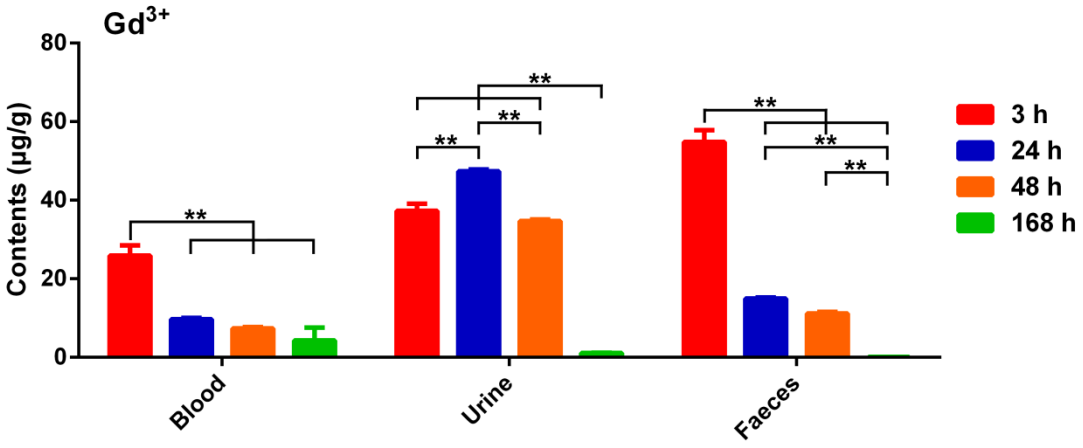

Figure S23. The dynamic change of Gd in blood, urine and faeces after i.v injection of AR-Bi@SiO_2-Gd. The data indicate that the targeted AR-Bi@SiO_2-Gd could be expeled from the body through urine and faeces after 7 days. *p < 0.05, **p < 0.01.

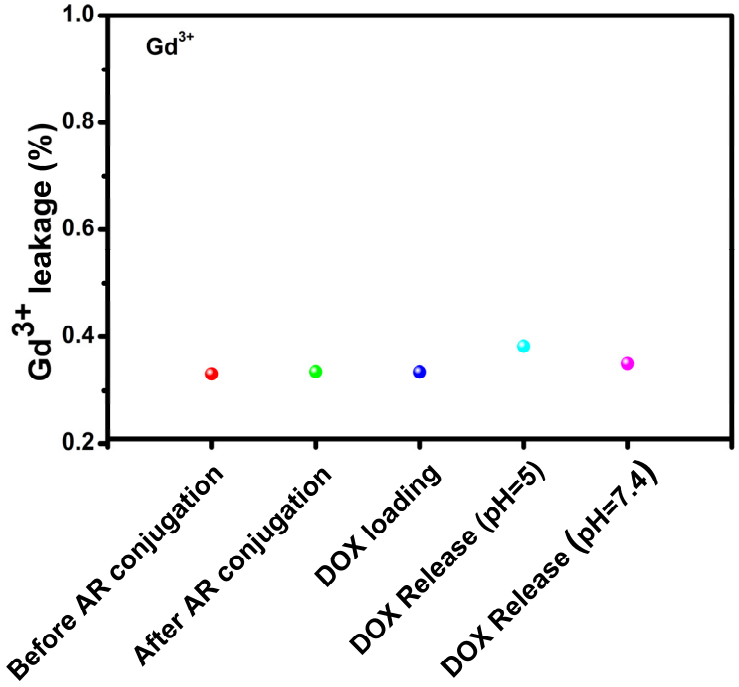

Figure S24. Gd^{3+} leakage from the AR-Bi@SiO_2-Gd during peptide conjugation, drug loading and drug release (pH=5, 7.4) process.

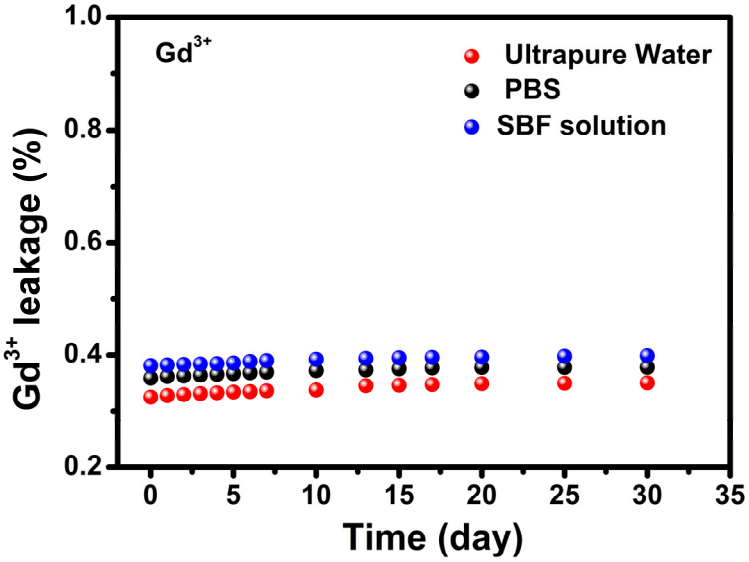

Figure S25. Gd^{3+} leakage from the Bi@SiO_2-Gd in different solutions during 30 days.

References

1. X. Qu, P. Qiu, Y. Zhu, M. Yang, C. Mao, *NPG Asia Mater*. 2017, **9**, e452.
2. B. Wei, X. Zhang, C. Zhang, Y. Jiang, Y.Y. Fu, C. Yu, S.K. Sun, X.P. Yan, *ACS Appl. Mater. Interfaces*, 2016, **8**, 12720.
3. L. Li, Y. Lu, C. Jiang, Y. Zhu, X. Yang, X. Hu, Z. Lin, Y. Zhang, M. Peng, H. Xia, C. Mao, *Adv. Funct. Mater*. 2018, **28**, 1704623